

d-Wave superconductivity as a catalyst for antiferromagnetism in underdoped cuprates

Markus Schmid, Brian M. Andersen, Arno P. Kampf, P. J. Hirschfeld

Angaben zur Veröffentlichung / Publication details:

Schmid, Markus, Brian M. Andersen, Arno P. Kampf, and P. J. Hirschfeld. 2010. "d-Wave superconductivity as a catalyst for antiferromagnetism in underdoped cuprates." *New Journal of Physics* 12 (5): 053043.
<https://doi.org/10.1088/1367-2630/12/5/053043>.

d-Wave superconductivity as a catalyst for antiferromagnetism in underdoped cuprates

To cite this article: Markus Schmid *et al* 2010 *New J. Phys.* **12** 053043

View the [article online](#) for updates and enhancements.

Related content

- [Disorder induced stripes in d-wave superconductors](#)
Markus Schmid, Florian Loder, Arno P Kampf *et al.*
- [Modeling of superconducting stripe phases in high-T_c cuprates](#)
F Loder, S Graser, M Schmid *et al.*
- [The t-J model for the oxide high-T_c superconductors](#)
Masao Ogata and Hidetoshi Fukuyama

Recent citations

- [Low-frequency quantum oscillations due to strong electron correlations](#)
A. Sherman
- [Impurity states and cooperative magnetic order in Fe-based superconductors](#)
Maria N. Gastiasoro *et al*

d-Wave superconductivity as a catalyst for antiferromagnetism in underdoped cuprates

Markus Schmid^{1,4}, Brian M Andersen², Arno P Kampf¹ and P J Hirschfeld³

¹ Theoretical Physics III, Center for Electronic Correlations and Magnetism, Institute of Physics, University of Augsburg, D-86135 Augsburg, Germany

² Niels Bohr Institute, University of Copenhagen, Universitetsparken 5, DK-2100 Copenhagen, Denmark

³ Department of Physics, University of Florida, Gainesville, FL 32611, USA
E-mail: markus.schmid@physik.uni-augsburg.de

New Journal of Physics **12** (2010) 053043 (17pp)

Received 3 February 2010

Published 26 May 2010

Online at <http://www.njp.org/>

doi:10.1088/1367-2630/12/5/053043

Abstract. In underdoped high- T_c cuprates, d-wave superconductivity competes with antiferromagnetism. It has generally been accepted that suppressing superconductivity leads to the nucleation of spin-density wave (SDW) order with wavevector near (π, π) . We show theoretically, for a d-wave superconductor in an applied magnetic field including disorder and electronic correlations, that the creation of SDW order is in fact not simply due to suppression of superconductivity, but rather due to a correlation-induced splitting of an electronic bound state arising from the sign change of the order parameter along quasiparticle trajectories. The induced SDW order is therefore a direct consequence of the d-wave symmetry. The formation of anti-phase domain walls proves to be crucial for explaining the heretofore puzzling temperature dependence of the induced magnetism as measured by neutron diffraction.

A superconductor is characterized by a Bardeen–Cooper–Schrieffer (BCS) order parameter $\Delta_{\mathbf{k}}(\mathbf{R})$, where \mathbf{R} is the center-of-mass coordinate of a Cooper pair of electrons with momenta $(\mathbf{k}, -\mathbf{k})$. The bulk ground state of such a system is homogeneous, but a spatial perturbation that breaks pairs, e.g. a magnetic impurity, may cause the suppression of $\Delta_{\mathbf{k}}(\mathbf{R})$ locally. What is revealed when superconductivity is suppressed is the electronic phase in the absence of $\Delta_{\mathbf{k}}$, a normal Fermi liquid. Thus the low-energy excitations near magnetic impurities and in the vortex

⁴ Author to whom any correspondence should be addressed.

cores of conventional superconductors are essentially Landau quasiparticles trapped in bound states. The underdoped cuprates have been studied intensively in recent years, in part because their proximity to the Mott insulator is thought to be responsible for many unusual properties, including possibly high-temperature superconductivity itself. These systems are quite different from conventional superconductors, because when the pair amplitude is suppressed locally, e.g. by a vortex, a competing ordered state [1] stabilized by the proximity to the Mott state appears to emerge instead of a normal metal. This state is characterized at low temperatures T by static local spin-density wave (SDW) order with an ordering wavevector \mathbf{Q} near (π, π) , an order that is not present in the state above T_c . This was first reported in elastic neutron scattering experiments [2] on $\text{La}_{2-x}\text{Sr}_x\text{CuO}_4$ (LSCO), with a correlation length of several hundred Angstrom (\AA), but has been confirmed in other underdoped cuprates as well [3–6]. An enhancement of incommensurate static order was observed on increasing the applied magnetic field up to 14 T [2]. Because the signal disappeared above T_c , the magnetism was attributed to the vortices; indeed, scanning tunneling microscopy (STM) measurements [7] on $\text{Bi}_2\text{Sr}_2\text{CaCu}_2\text{O}_{8+\delta}$ (BSSCO) were able to directly image unusual charge order near the vortex cores, which is almost certainly related to the field-induced SDW detected by neutron scattering.

Signatures of antiferromagnetic (AF) ordering in the SC state had been found earlier by nuclear magnetic resonance (NMR) experiments [8]. Subsequently, μSR experiments [9, 10] detected magnetic ordering as a wedge-shaped extension of the ‘spin glass’ phase into the SC dome of the temperature versus doping phase diagram (figure 1(a)). Lake *et al* [2] reported that an incommensurate magnetic order similar to the field-induced state was also observed in zero field. Although it also vanished at T_c , the ordered magnetic moment in zero field had a T dependence, which was qualitatively different from the field-induced signal. The zero-field signal was attributed to disorder, but the relation between impurities and magnetic ordering remained unclear. Because strong magnetic fluctuations with similar wavevectors are reported at low but nonzero energies in inelastic neutron scattering experiments on these materials, e.g. on optimally doped LSCO samples exhibiting no spin-glass phase in zero field, it is frequently argued that impurities or vortices simply ‘freeze’ this fluctuating order [11].

Describing such a phenomenon theoretically at the microscopic level is difficult due to the inhomogeneity of the interacting system, but it is important if one wishes to explore situations with strong disorder, where the correlations may no longer reflect the intrinsic spin dynamics of the pure system. Such an approach was proposed in a model calculation for an inhomogeneous d-wave superconductor with Hubbard-type correlations treated in the mean field [12]. In this model, a single impurity creates, at sufficiently large Hubbard interaction U and impurity potential strength V_{imp} , a droplet of staggered magnetization with a size corresponding to the AF correlation length of the hypothetical pure system [13–16]. When these droplets come close enough to interact, there is a tendency to form incommensurate, phase-coherent Néel domains whose size is sufficient to explain the observations by Lake *et al* [2] in zero field [12]. Such a model explains the empirical observations that both increasing disorder [17] and underdoping [9] enhance the SDW order.

In this paper, we investigate the origin of the ‘order by disorder’ phenomenon described in [12], as well as the T evolution of the disordered magnetic state in applied magnetic field. An apparently very natural approach to the problem was developed by Demler *et al* [18], who constructed a Ginzburg–Landau (GL) theory for competing SDW and SC order in a magnetic field. This phenomenology describes correctly the reduction of condensation energy in the vortex phase of the pure superconductor, and leads to a phase diagram qualitatively

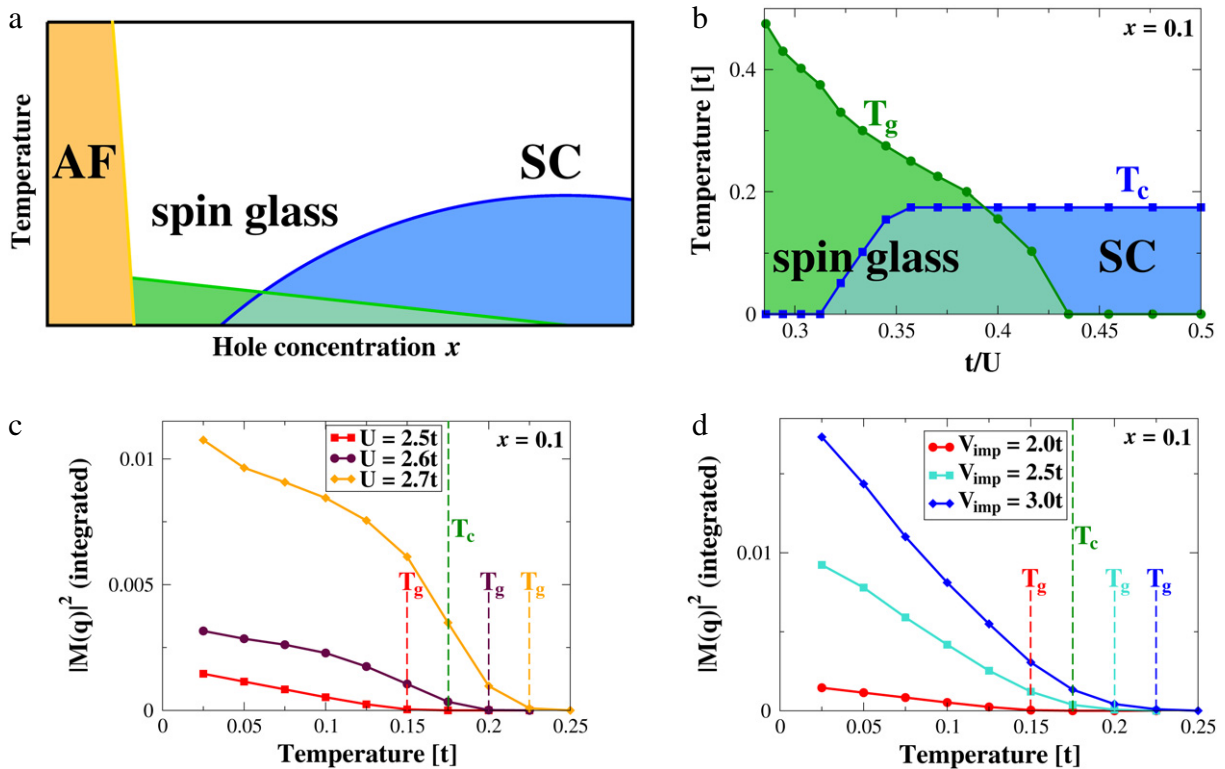


Figure 1. Phase diagrams and temperature dependence of magnetic order. (a) Schematic temperature T versus doping x -phase diagram for cuprates. (b) t/U dependence of the SC T_c and the disorder-induced magnetic transition temperature T_g for an impurity concentration $n_{\text{imp}} = 10\%$ with potential strength $V_{\text{imp}} = 2.0t$ and a hole concentration $x = 0.1$. t is the nearest-neighbor hopping amplitude and U denotes the Hubbard on-site repulsion. (c, d) Magnetic Fourier component $|M(\mathbf{q})|^2$ at the ordering wavevector integrated around (π, π) versus temperature for (c) different interaction strengths U (at fixed $V_{\text{imp}} = 2.0t$) and (d) different impurity potential strengths V_{imp} (at fixed $U = 2.5t$).

consistent with experiments [1]. But it ignores the energies of the quasiparticles moving in the inhomogeneous state, which can also crucially affect the competition between SDW and SC order at low T , as we show here.

In a d-wave superconductor without AF correlations, a bound state of an isolated vortex is found at zero energy [19] due to the sign change of the order parameter on quasiparticle trajectories through the vortex core. On the other hand, solutions of the Bogoliubov–de Gennes (BdG) equations describing coexisting d-wave superconductivity and SDW order [20–24] show that this resonance is split by the SDW formation; that is, the system can lower the energy of the nearly bound quasiparticles by moving them below the Fermi energy. This finding is consistent with the STM experiments in the Abrikosov state of $\text{YBa}_2\text{Cu}_3\text{O}_{7-\delta}$ (YBCO) [25] and of BSCCO [26], in which split peaks were observed in the vortex cores. A similar bound state is associated with non-magnetic impurities such as Zn in BSCCO and was also imaged by STM [27]. It is therefore important to explore the role of quasiparticle bound states and their coupling to the SDW order to identify the origin of both types of induced local AF in the SC

state. An understanding of field-induced order is also highly relevant for the interpretation of the quantum oscillations observed in recent transport experiments in high magnetic fields [28, 29], since oscillations are possibly due to the formation of Fermi surface pockets as a consequence of SDW ordering.

The inhomogeneous mean-field theory presented here for electrons hopping on a square lattice with a d-wave pairing potential and subject to a Hubbard on-site repulsion U reproduces the essential aspects of the field-induced spin-glass phase shown schematically in figure 1(a). If doping is assumed to be correlated with the ratio of bandwidth to local Coulomb repulsion, a phase diagram very much like the one found in various cuprate materials is obtained (see figures 1(b)–(d)). We consider this a reasonable qualitative approach, since the reported changes in the Fermi surface of these materials over the ‘spin-glass’ doping range are small [30] and it is therefore plausible that the primary effect on the electronic structure is due to the correlation-induced band narrowing [12]. The magnetically ordered phase can be enhanced by the increase in the correlation strength or stronger disorder potentials (see figures 1(c) and (d)).

Our results reproduce well the qualitative aspects of the experiment by Lake *et al* [2]. We find that some features depend on nonuniversal aspects of disorder, in particular the process of domain wall nucleation, and that while disorder- and magnetic-field-induced SDW order both add to the ordered moment, the interference of disorder and magnetic-field effects is quantitatively significant. The domain wall formation proves to be responsible for the distinct T dependences of the field- and the disorder-induced magnetization. The present theory also includes a crossover from magnetic droplets to filamentary stripe-like structures in selected regimes of hole densities and impurity concentrations. The model therefore offers a route to describe the physics of the pinning of stripe correlations in the SC state. This insight may prove relevant for many experiments in the underdoped cuprates that have been attributed to stripes.

The basis for our model analysis is the pairing Hamiltonian for a d-wave superconductor with orbital coupling to an applied magnetic field \mathbf{B} , to which we add site-centered disorder and a local Hubbard repulsion; the latter is treated in an unrestricted Hartree–Fock approximation:

$$H = - \sum_{ij\sigma} t_{ij} e^{i\varphi_{ij}} c_{i\sigma}^\dagger c_{j\sigma} - \mu \sum_{i\sigma} c_{i\sigma}^\dagger c_{i\sigma} + \sum_{\langle ij \rangle} \left(\Delta_{ij} c_{i\uparrow}^\dagger c_{j\downarrow}^\dagger + \text{h.c.} \right) + \frac{U}{2} \sum_i \left(\langle n_i \rangle n_i - \langle \sigma_i^z \rangle \sigma_i^z \right) + \sum_{i\sigma} V_i^{\text{imp}} c_{i\sigma}^\dagger c_{i\sigma}. \quad (1)$$

Here, $c_{i\sigma}^\dagger$ creates an electron on a square lattice site i with spin $\sigma = \uparrow, \downarrow$. The hopping matrix elements between nearest and next-nearest neighbor sites are denoted by $t_{ij} = t$ and $t_{ij} = t'$, respectively. An electron moving in the magnetic field from site j to i acquires additionally the Peierls phase $\varphi_{ij} = (\pi/\Phi_0) \int_{\mathbf{r}_j}^{\mathbf{r}_i} \mathbf{A}(\mathbf{r}) \cdot d\mathbf{r}$, where $\Phi_0 = hc/(2e)$ and $\mathbf{A}(\mathbf{r}) = B(0, x)$ is the vector potential in the Landau gauge. The chemical potential μ is adjusted to fix the electron density $n = \frac{1}{N} \sum_i \langle n_i \rangle = 1 - x$, where x is the hole concentration; in the following we will focus on $x = 0.1$. The d-wave pairing amplitude Δ_{ij} is determined by the strength of an attractive nearest-neighbor interaction V_d . The non-magnetic impurity potential V_i^{imp} consists of a set of point-like scatterers at random positions, and all fields, i.e. Δ_{ij} , the local charge density $\langle n_i \rangle$ and the local magnetization $\langle \sigma_i^z \rangle$ are calculated self-consistently from the solutions of the associated BdG equations. (For further details see the [appendix](#).)

We start with a single impurity in a d-wave superconductor at $U = 0$. The fingerprint of the induced virtual bound state is a single near-zero-energy peak in the local density of states

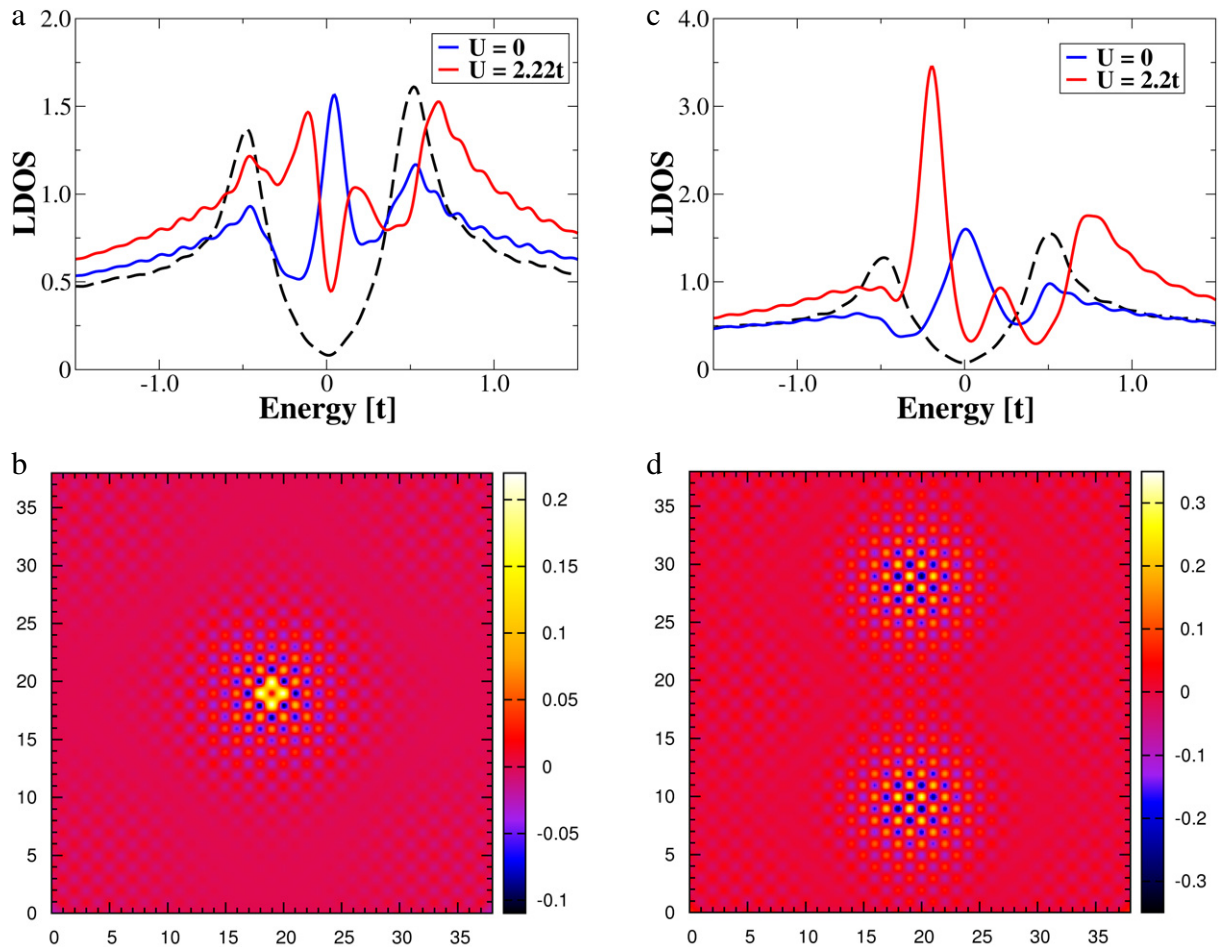


Figure 2. Impurity- and field-induced magnetization. (a, c) LDOS at a nearest-neighbor site of a single impurity ($V_{\text{imp}} = 60t$) (a) and in the center of one vortex (c). In both cases, above a critical U_c , local SDW order is induced; concomitantly the zero-energy peak in the absence of the Hubbard repulsion (blue curve) splits spin dependently (red curve). The dashed curves show the clean LDOS far from the perturbation. (b, d) Real-space patterns of the magnetization $\langle \sigma_i^z \rangle$ in units of μ_B on a 38×38 lattice for $U = 2.2t > U_c$ at low temperature $T = 0.025t$. (b) shows the magnetization nucleated by a strong impurity ($V_{\text{imp}} = 60t$) located at the center. In (d) two superconducting flux quanta $\Phi = 2\Phi_0$ thread an impurity-free d-wave superconductor.

(LDOS) (figure 2(a)), and no magnetization is induced by the impurity. Increasing the Hubbard repulsion beyond a critical value U_c , a staggered magnetization emerges in the neighborhood of the impurity (figure 2(b)). The two-sublattice nature of the magnetic pattern, in conjunction with the spatial extent of the impurity resonance, leads to a spin-dependent splitting of the peak in the LDOS; one resonant state with a selected spin direction is thereby shifted below and the other above the Fermi energy, as is most clearly seen at the nearest-neighbor sites of the impurity (figure 2(a)). The spin-dependent splitting reduces the bound-state energy of a spin-up or -down state, and therefore stabilizes a local droplet of staggered magnetization, which carries a total

spin-1/2 moment. The splitting of the resonance peak can therefore be viewed as the origin of the impurity-induced magnetization. It is important to note that the splitting of the bound state is *not* due to the suppression of the d-wave order parameter near the impurity. As we have verified, the order parameter can be artificially held constant in the solution of the BdG equations, and a nearly identical result is obtained.

For a finite density of impurities, we recover at $T = 0$ the results of [12], i.e. the creation of a defective but magnetically ordered state as defined by strong peaks in the Fourier transform of the local magnetization $M(\mathbf{q})$ at incommensurate wavevectors \mathbf{q} near (π, π) . The effect of temperature is now naturally included in the theory via T -dependent occupation probabilities of Bogoliubov quasiparticle states. In figure 1(b), we show the extent of the quasi-ordered phase, labeled ‘spin glass’, which expands as correlations increase, and disappears at a critical value of t/U , which depends on the strengths of the pairing interaction and the impurity potential. The intensity of the incommensurate magnetic Bragg peaks is shown in figures 1(c) and (d) as functions of T for fixed t/U and fixed impurity potential strength, respectively. From figure 1(c) it becomes evident that the magnetic ordering or ‘glass transition’ temperature T_g can be smaller, equal to or larger than T_c depending on U . Increasing the impurity potential V_{imp} can increase both the amplitude of the disorder-induced SDW and T_g itself (figure 1(d)). These results are consistent with the empirical observation that the size of the spin-glass phase is not universal, and in particular the critical doping beyond which magnetic order is no longer observed varies considerably between intrinsically disordered cuprates, such as LSCO and BSCO, and clean materials, like YBCO.

The magnetization induced by an orbital magnetic field can be traced to the same microscopic origin as the impurity-induced magnetization [21]. Above a critical U_c , a staggered spin pattern is nucleated in the vortex cores with a spatial extent reaching beyond the size of a vortex core (figure 2(d)), as observed in experiment [2]. For the parameter set chosen, the core radius estimated from the area where the order parameter is suppressed is about one lattice spacing. The LDOS in the vortex center reveals that the origin of the field-induced magnetization is tied to the spin-dependent splitting of the Andreev bound state in the vortex core (figure 2(c)). The conjecture that the field-induced magnetization indeed appears simultaneously with the peak splitting in the LDOS is explicitly verified in figure 3. For the unmagnetized vortex at $T = 0.175t$, a single Andreev bound-state peak exists at zero energy. With decreasing T , the vortices nucleate a staggered spin pattern precisely when the zero-energy peak in the LDOS splits. With further cooling the peak splitting grows, more spectral weight is shifted below the Fermi energy and the magnetization is enhanced.

The natural next step is to consider a finite density of non-magnetic impurities in the presence of an external magnetic field and to compare it with the zero-field results. Specifically for the modeling of LSCO, we assume in the following that the Sr ions are the primary source of disorder, such that x equals the impurity concentration n_{imp} . These systems are in the strongly disordered regime where the AF correlation length (droplet size) is comparable to the average distance between the dopants. Since the Sr dopants are removed from (but close to) the CuO_2 planes, we model them as weak scatterers with $V_{\text{imp}} = 1.3t$. Figures 4(a) and (b) show the averaged magnetic structure factor $S(\mathbf{q})$ at a fixed temperature far below T_c in zero and finite magnetic field. As in figures 1(c) and (d), $S(\mathbf{q})$ is approximated by $|M(\mathbf{q})|^2$ with $M(\mathbf{q}) = \frac{1}{N} \sum_i e^{i\mathbf{q}\cdot\mathbf{r}_i} \langle \sigma_i^z \rangle$. The magnetic signal in the structure factor appears at the incommensurate wavevectors $\mathbf{q} = (\pi, \pi \pm \delta)$ and $\mathbf{q} = (\pi \pm \delta, \pi)$ (figure 4(a)). δ , however, varies for randomly selected impurity configurations. For the weak magnetic signal in zero field,

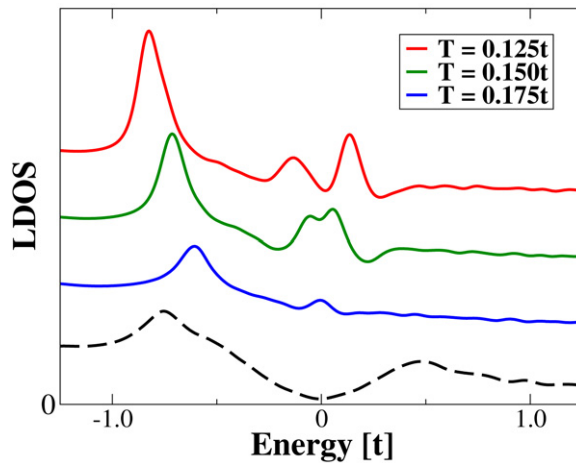


Figure 3. Temperature-dependent peak splitting in a magnetic field. LDOS at the vortex center for three different temperatures below T_c in the absence of impurities. Below the critical temperature $T_g = 0.175t$, the vortices magnetize and simultaneously the Andreev bound-state peak splits. The black dashed curve shows the LDOS far away from the vortex.

the averaging over different impurity configurations is therefore imperative but computationally demanding. Applying an external magnetic field strongly enhances the magnetization and reinforces incommensurate peaks at unambiguous wavevectors that are robust against variations in the impurity configurations (figure 4(b)).

Remarkably, the temperature dependence of the structure factor (figure 4(c)) closely resembles the neutron scattering data on LSCO by Lake *et al* [2]. For the results shown in figure 4, we have chosen a parameter set where the staggered magnetization in zero field has its onset at a temperature T_g indistinguishable from T_c . This reflects a situation where, upon cooling through T_c , the localized bound states inside the d-wave energy gap emerge and immediately split in the self-stabilizing staggered magnetic pattern. Towards lower T the magnetic structure factor rises in a markedly different way in zero and in finite field. While the field-induced part of the magnetic signal has a negative curvature, the zero field $S(\mathbf{q})$ increases approximately linearly upon cooling. The two mechanisms of impurity- and field-induced SDW do not simply cooperate additively; the field-induced part is twice as large in the presence of impurities as compared with the field-induced magnetization in the clean system (figure 4(c)). The zero-field increase of the magnetization in the inhomogeneous SC state originates from the merging of AF patches nucleated by the individual impurities. Without impurities the increasing field-induced magnetization with cooling results from the growth of the magnetized regions around the well-separated vortex cores. Thus, both our zero- and finite-field results for the finite density of impurities $n_{\text{imp}} = x$ closely follow the T dependence of the neutron scattering data for underdoped LSCO [2]. Still, due to computational restrictions, we are not yet able to access the low magnetic-field strengths to allow for a direct comparison with experiment.

An important remaining question is why the T dependences of the magnetization are different in zero and in finite field. A hint is provided by the observation that the T dependence of the magnetic structure factor for the impurity-free field-induced magnetization and also for just two single impurities in zero field has a negative curvature. In both cases, the induced

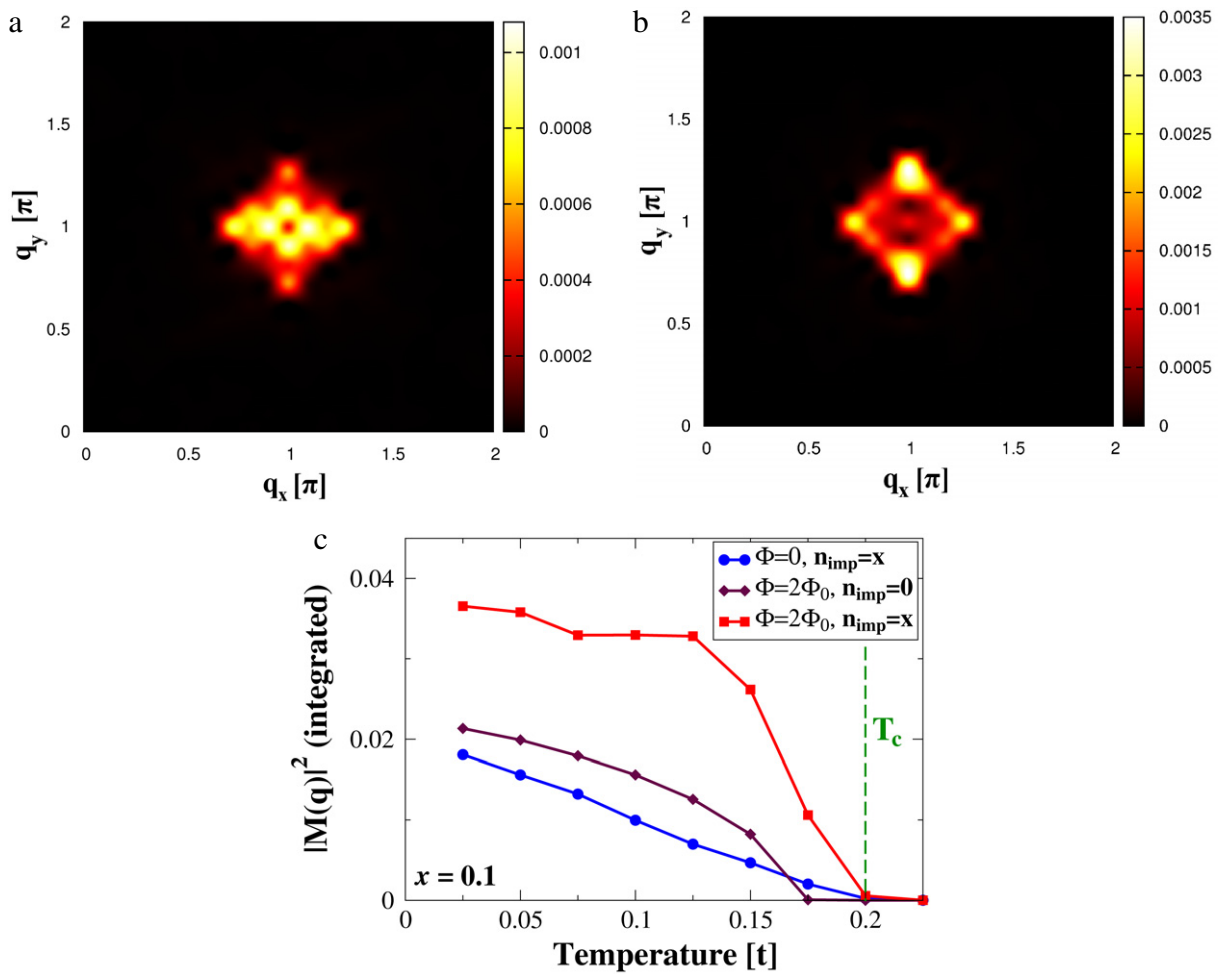


Figure 4. Averaged magnetic structure factor for a many-impurity system. (a, b) Intensity plot of the magnetic structure factor around (π, π) at $T = 0.025t$ in zero magnetic field (a) and at finite field (b). The structure factor data were averaged over ten different impurity configurations. For the used system size of 22×22 lattice sites, a magnetic flux of $2\Phi_0$ corresponds to a strong magnetic field with $H = 59 T$. The impurity concentration $n_{\text{imp}} = x$ is fixed to 10% ($V_{\text{imp}} = 1.3t$) and $U = 2.9t > U_c$. (c) T dependence of the peak intensity integrated around (π, π) in zero field and at finite field with the finite density of impurities $n_{\text{imp}} = x$ (blue and red curves, respectively); for the data with $\Phi = 2\Phi_0$ and $n_{\text{imp}} = x$, the zero-field data were subtracted. For comparison, the structure factor in a clean system is also included for the same magnetic-field strength (purple curve). $|M(\mathbf{q})|^2$ (integrated) translates directly to the ordered spin moment squared in units of μ_B per Cu^{2+} .

staggered magnetization patterns around each impurity or each vortex, respectively, adjust their individual two-sublattice spin structures in phase and thereby avoid domain walls [31]. For three nearby impurities, however, it already proves difficult to find a specific configuration where anti-phase domain walls are absent. In figures 5(a) and (b), we compare two three-impurity configurations with distinctly different domain-wall patterns. Remarkably, placing the three

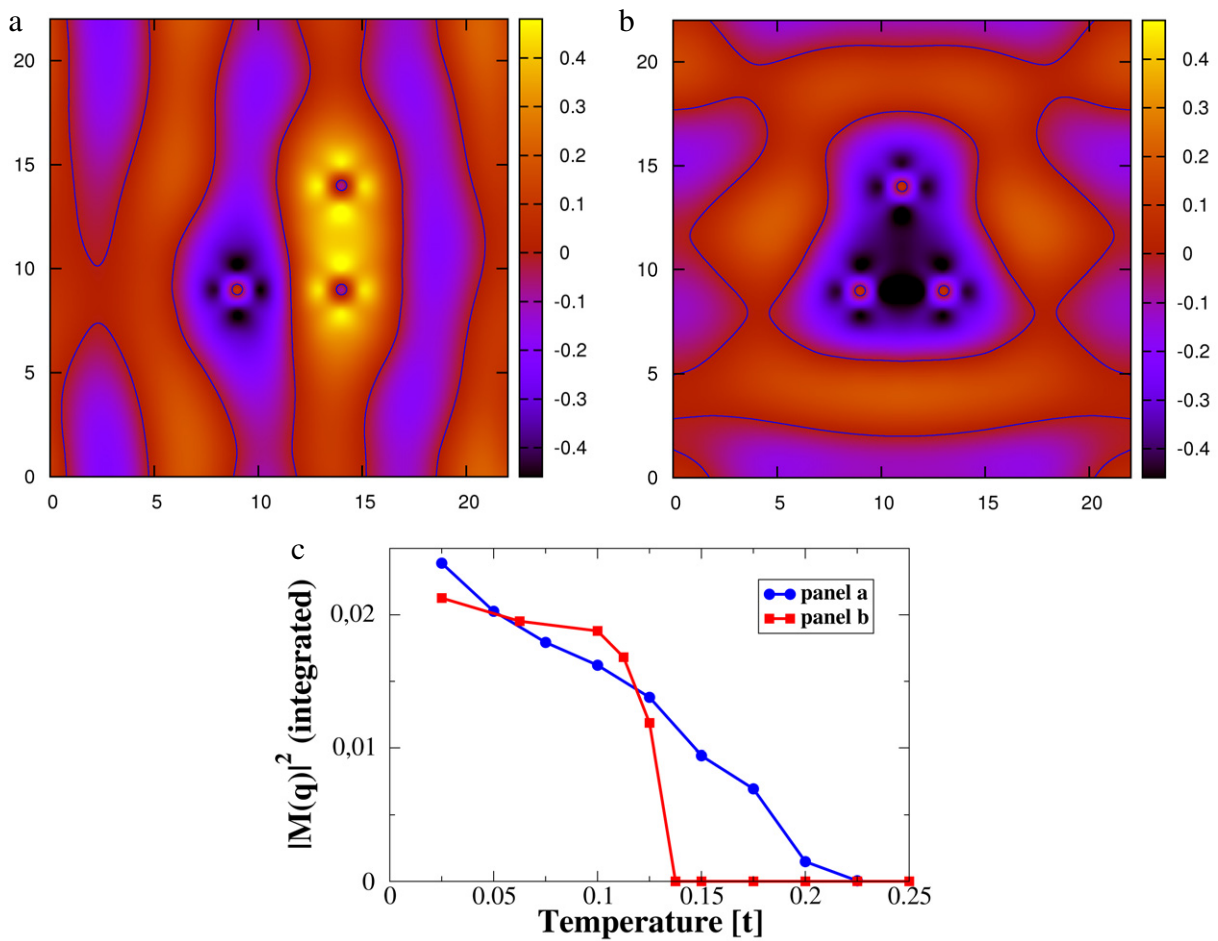


Figure 5. Anti-phase domain walls. (a, b) Real-space image of the staggered magnetization at $T = 0.025t$ induced by three non-magnetic impurities. In impurity configuration, (a) anti-phase domain walls appear vertically. In configuration (b), the staggered magnetization induced by the three impurities adjusts to a uniform AF domain around them. (c) Temperature dependence of the integrated magnetic structure factor for the impurity configurations (a) (blue curve) and (b) (red curve), respectively.

impurities on the same sublattice to form a right-angled isosceles triangle, as in figure 5(a), generates a sequence of vertical anti-phase domain walls. If instead the impurities are configured in an acute isosceles triangle, as in figure 5(b), a simply connected AF island forms around them. As figure 5(c) shows, with decreasing T the magnetic signal evolves differently for each impurity configuration. Intriguingly, $|M(\mathbf{q})|^2$ rises almost linearly for the configuration with vertical anti-phase domain walls while it has a negative curvature for the single domain island. These examples suggest that the linear low- T rise of the magnetic signal for a finite density of impurities in zero field originates from the anti-phase domain walls that are always present in the randomly generated impurity configurations. For the field-induced magnetization, it is the larger distance between the magnetized vortices that prevents the occurrence of domain walls and therefore alters the T dependence of $|M(\mathbf{q})|^2$.

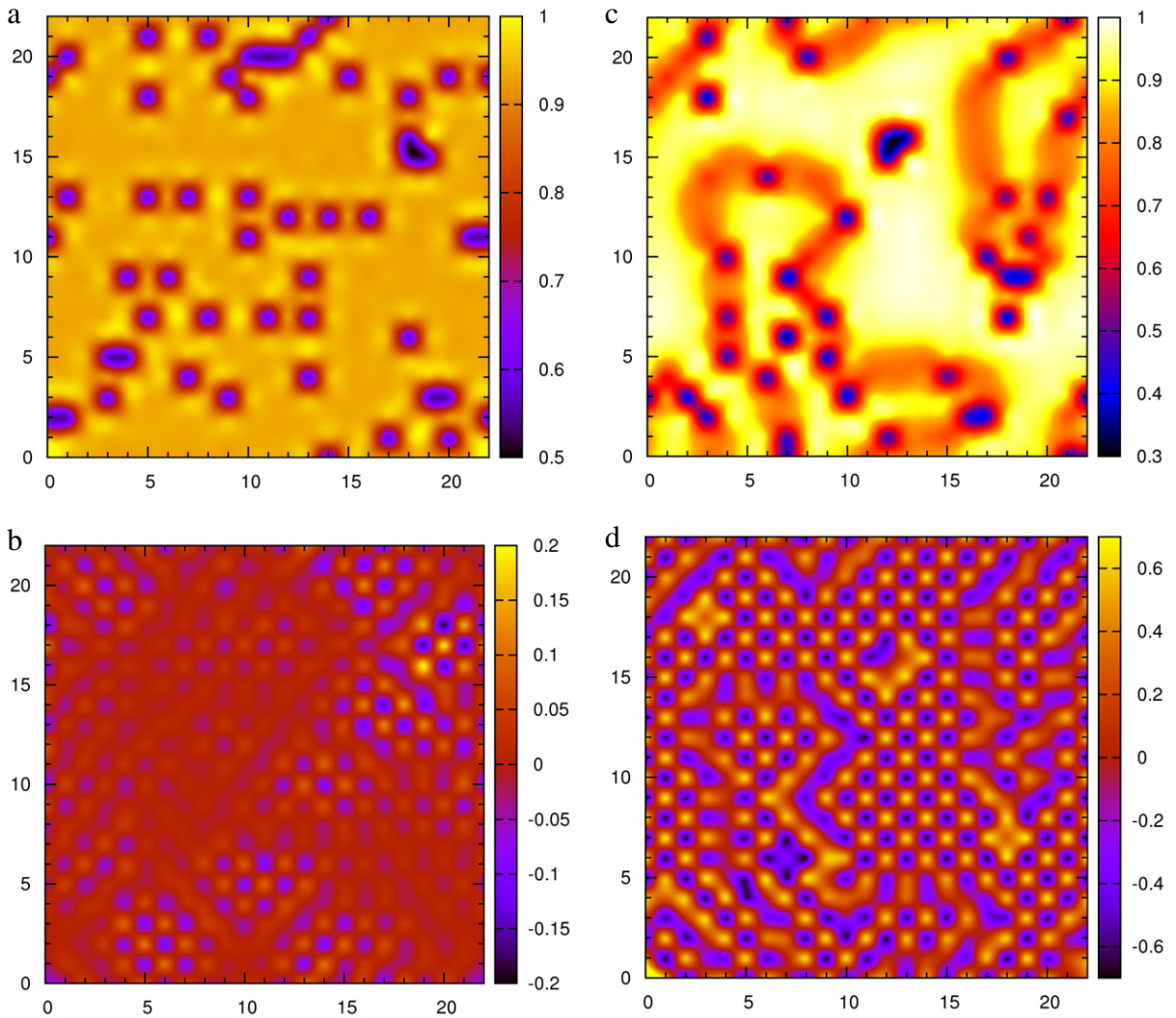


Figure 6. (a, c) Charge-density profiles. (b, d) Magnetization. (a, b) The same parameter set in zero field as in figure 4: $U = 2.9t$, doping $x = 10\% = n^{\text{imp}}$ and pairing interaction strength $V_d = 1.34t$. (c, d) $U = 4.0t$, doping $x = 15\%$, $n^{\text{imp}} = 7.5\%$ and $V_d = 2.0t$. In (a–d) the temperature is fixed to $T = 0.025t$ and $V_{\text{imp}} = 1.3t$.

The results presented above focused on static disorder- and field-induced SDW, but inelastic neutron scattering experiments have shown that in the SC state the spin excitations at finite energy have almost the same distribution of spectral weight in \mathbf{q} as the frozen magnetic order (for a review see [32]). Thus in the SC state, where our model is applicable, we have provided a concrete foundation for the freezing of fluctuating spin correlations by disorder and magnetic field on the same footing; in particular, the role of the quasiparticle bound states in the formation of the magnetic order has been highlighted.

The new picture that emerges is complementary to the global competition between SC and AF phases in the sense that superconductivity and disorder may significantly enhance SDW order in the underdoped regime. The d-wave pairing of the SC condensate is crucial for this

generation of local magnetism, as we have shown. Support for this cooperative effect between SDW and superconductivity comes not only from the onset of the elastic magnetic neutron signal at T_c but also from Zn-substituted optimally doped LSCO. There it is found by μ SR that 2% Zn induces a magnetic signal, but 3% Zn is found to eliminate it, but also destroys superconductivity [33]; within the context of the current theory, this effect is understood not as a consequence of spin dilution [33], but rather due to the destruction of the SC phase and thereby its ability to generate (or enhance) magnetic order via bound state creation. Similar effects were observed at smaller Zn concentrations in underdoped LSCO samples [34].

Finally, we show that a qualitatively different kind of inhomogeneous texture may also be stabilized within the present weak-coupling approach. Figures 6(a) and (b) show the typical charge-density profile and the corresponding magnetization in zero field for the parameter set used above to explore the onset of static AF order. As expected, the electron density is reduced at the impurity sites, and local SDW patches nucleate around them. With increasing repulsion U and for hole densities that exceed the impurity concentration, the inhomogeneous spin and charge patterns change qualitatively (see figures 6(c, d)). The magnetically ordered patches evolve to connected strongly magnetized areas separated by hole-rich filamentary structures serving as anti-phase domain walls. In this still SC state the filaments constitute snake-like paths through an SDW background with an average density of almost one electron per site. These textures provide a link to the study of disordered (quenched) stripes similar to those discussed recently within various GL models [35–37]. Therefore, depending upon the correlation strength and the details of the disorder, the magnetic ordering temperature T_g can vary significantly, and the ordering itself can be droplet or filamentary-like. This may explain many of the differences of neutron and μ SR experiments on different cuprate families at various doping levels.

Acknowledgments

This work was supported by the DFG through SFB 484 (MS and APK), by The Danish Council for Independent Research | Natural Sciences (BMA) and by the DOE under grant DE-FG02-05ER46236 (PJH).

Appendix. Numerical method

In order to investigate disorder- and field-induced magnetic order in d-wave superconductors, we self-consistently solve the BdG equations on a square lattice for the Hamiltonian

$$\begin{aligned}
 H = & - \sum_{ij\sigma} t_{ij} e^{i\varphi_{ij}} c_{i\sigma}^\dagger c_{j\sigma} - \mu \sum_{i\sigma} c_{i\sigma}^\dagger c_{i\sigma} + \sum_{(ij)} \left(\Delta_{ij} c_{i\uparrow}^\dagger c_{j\downarrow}^\dagger + \text{h.c.} \right) \\
 & + \frac{U}{2} \sum_i (\langle n_i \rangle n_i - \langle \sigma_i^z \rangle \sigma_i^z) + \sum_{i\sigma} V_i^{\text{imp}} c_{i\sigma}^\dagger c_{i\sigma},
 \end{aligned} \tag{A.1}$$

where the hopping amplitude between nearest-neighbor and next-nearest-neighbor sites i and j is described by $t_{ij} = t$ and $t_{ij} = t' = -0.4t$, respectively. An orbital magnetic field is represented by the Peierls phase factor $\varphi_{ij} = (\pi/\Phi_0) \int_{\mathbf{r}_j}^{\mathbf{r}_i} \mathbf{A}(\mathbf{r}) \cdot d\mathbf{r}$, while $\Phi_0 = hc/(2e)$ is the superconducting flux quantum and $\mathbf{A}(\mathbf{r}) = (0, Bx)$ is the vector potential of the magnetic field

in the Landau gauge. The d-wave pairing potential is defined on two nearest-neighbor sites i and j by

$$\Delta_{ij} = -V_d \langle c_{j\downarrow} c_{i\uparrow} \rangle = \Delta_{ji}, \quad (\text{A.2})$$

where V_d is the attractive pairing interaction strength, which we set to $V_d = 1.34t$ throughout the paper. We then define a gauge invariant d-wave order parameter on each lattice site i :

$$\Delta_i^d = \frac{1}{4} \left(\Delta_{i,i+\hat{x}}^d + \Delta_{i,i-\hat{x}}^d - \Delta_{i,i+\hat{y}}^d - \Delta_{i,i-\hat{y}}^d \right), \quad (\text{A.3})$$

where $\Delta_{i,j}^d = \Delta_{ij} \exp[-i(\pi/\Phi_0) \int_{\mathbf{r}_j}^{\mathbf{r}_i} \mathbf{A}(\mathbf{r}) \cdot d\mathbf{r}]$. The chemical potential μ is adjusted to fix the average charge density $n = \frac{1}{N} \sum_i \langle n_i \rangle$, while the electron number operator for spin σ at site i is given by $n_{i\sigma} = c_{i\sigma}^\dagger c_{i\sigma}$, and the local charge-density operator by $n_i = n_{i\uparrow} + n_{i\downarrow}$, $S_i^z = \frac{1}{2} \sigma_i^z = \frac{1}{2} (n_{i\uparrow} - n_{i\downarrow})$ is the z -component of the spin operator at site i .

The Bogoliubov transformation

$$c_{i\sigma} = \sum_n \left(u_{in\sigma} \gamma_{n\sigma} + v_{in\sigma}^* \gamma_{n-\sigma}^\dagger \right) \quad (\text{A.4})$$

diagonalizes the Hamiltonian in equation (A.2), which thereby takes the form

$$H = E_0 + \sum_{n\sigma} E_{n\sigma} \gamma_{n\sigma}^\dagger \gamma_{n\sigma}. \quad (\text{A.5})$$

E_0 is the ground-state energy and $\gamma_{n\sigma}^\dagger$ creates an elementary fermionic Bogoliubov quasiparticle excitation with quantum number n , spin σ and energy $E_{n\sigma} > 0$. Calculation of the commutators of H from equation (A.5) with the electron operators $c_{i\sigma}$ leads to a Schrödinger-like set of BdG equations

$$\sum_j \begin{pmatrix} H_{ij}^+ & \Delta_{ij} \\ \Delta_{ij}^* & -H_{ij}^{-*} \end{pmatrix} \begin{pmatrix} u_{jn\uparrow} \\ v_{jn\downarrow} \end{pmatrix} = E_{n\uparrow} \begin{pmatrix} u_{in\uparrow} \\ v_{in\downarrow} \end{pmatrix} \quad (\text{A.6})$$

and

$$\sum_j \begin{pmatrix} H_{ij}^+ & \Delta_{ij} \\ \Delta_{ij}^* & -H_{ij}^{-*} \end{pmatrix} \begin{pmatrix} v_{jn\uparrow}^* \\ u_{jn\downarrow}^* \end{pmatrix} = -E_{n\downarrow} \begin{pmatrix} v_{in\uparrow}^* \\ u_{in\downarrow}^* \end{pmatrix}, \quad (\text{A.7})$$

with

$$H_{ij}^\pm = -t_{ij} + \delta_{ij} \left[-\mu + \frac{U}{2} (\langle n_i \rangle \mp \langle \sigma_i^z \rangle) + V_i^{\text{imp}} \right]. \quad (\text{A.8})$$

As we only search for solutions with positive $E_{n\sigma}$, it is sufficient to solve the following single matrix equation:

$$\sum_j \begin{pmatrix} H_{ij}^+ & \Delta_{ij} \\ \Delta_{ij}^* & -H_{ij}^{-*} \end{pmatrix} \begin{pmatrix} u_{jn} \\ v_{jn} \end{pmatrix} = E_n \begin{pmatrix} u_{in} \\ v_{in} \end{pmatrix}. \quad (\text{A.9})$$

This is because the solutions for $E_n > 0$ are obviously identical to the solutions for the (positive) eigenvalues $E_{n\uparrow}$ of equation (A.6)

$$E_n > 0: \quad \begin{pmatrix} u_{in\uparrow} \\ v_{in\downarrow} \end{pmatrix} = \begin{pmatrix} u_{in} \\ v_{in} \end{pmatrix} \quad \text{and} \quad E_{n\uparrow} = E_n > 0, \quad (\text{A.10})$$

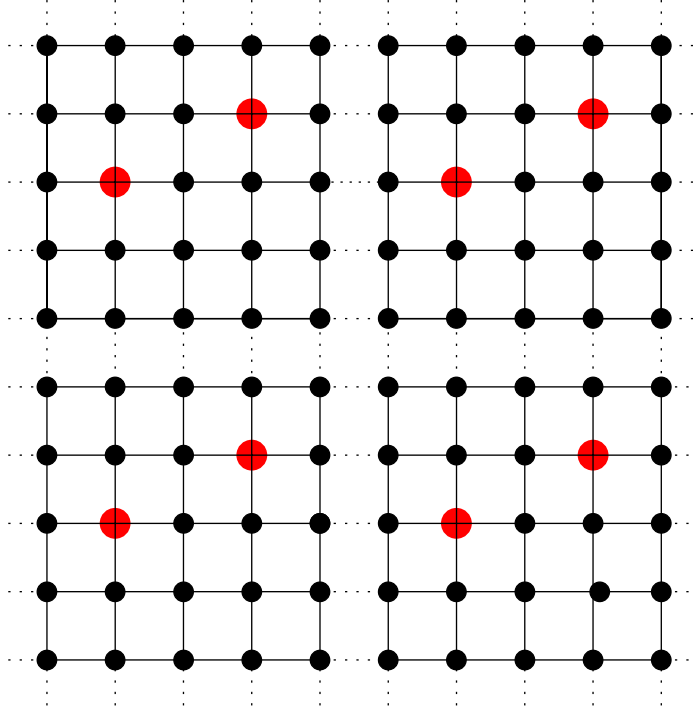


Figure A.1. Division of the lattice into identical supercells. Lattice sites belonging to the same supercell are connected via solid lines, whereas dashed lines link sites of different supercells. Red lattice sites simulate a possibly existing disorder.

while for $E_n < 0$ the following relation holds:

$$E_n < 0: \quad \begin{pmatrix} v_{in\uparrow}^* \\ u_{in\downarrow}^* \end{pmatrix} = \begin{pmatrix} u_{in} \\ v_{in} \end{pmatrix} \quad \text{and} \quad E_{n\downarrow} = -E_n > 0. \quad (\text{A.11})$$

Since the solutions of equations (A.6) and (A.7) can be mapped onto those of the BdG equation (A.9), we diagonalize equation (A.9) to obtain the pairing potential Δ_{ij} , the charge density $\langle n_i \rangle$ and the local magnetization $\langle \sigma_i^z \rangle$ self-consistently from

$$\Delta_{ij} = \frac{V_d}{4} \sum_n (u_{in} v_{jn}^* + u_{jn} v_{in}^*) \tanh\left(\frac{E_n}{2k_B T}\right), \quad (\text{A.12})$$

$$\langle n_{i\uparrow} \rangle = \sum_n |u_{in}|^2 f(E_n), \quad (\text{A.13})$$

$$\langle n_{i\downarrow} \rangle = \sum_n |v_{in}|^2 (1 - f(E_n)), \quad (\text{A.14})$$

$$\langle \sigma_i^z \rangle = \langle n_{i\uparrow} \rangle - \langle n_{i\downarrow} \rangle, \quad (\text{A.15})$$

where $f(E_n) = (1 + e^{E_n/k_B T})^{-1}$ is the Fermi distribution function and T is the temperature. Sums over n run over positive and negative energies E_n .

To maximize the size of the system for which equation (A.9) can be diagonalized numerically, we take advantage of the magnetic translation symmetry of our model Hamiltonian

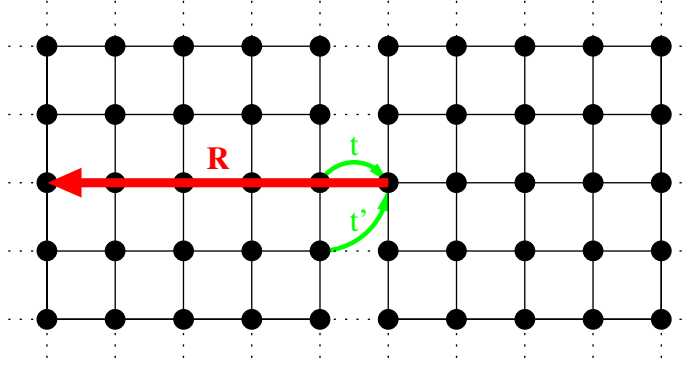


Figure A.2. Hopping between supercells. A particle, which hops from the left supercell into the right supercell, is mapped back to the left supercell through the translation vector \mathbf{R} . As a result the wave functions u and v obtain an additional phase given by the magnetic Bloch theorem equation (A.17).

equation (A.1) by dividing the lattice into $M_x \times M_y$ identical supercells each with $N_x \times N_y$ sites (see figure A.1) [21, 38, 39]. We define the following magnetic translation operator [40]:

$$\mathcal{T}_{\mathbf{R}} = \exp\left(-i \mathbf{R} \cdot \left(\mathbf{k} + \frac{q}{c\hbar} \mathbf{A}\right)\right), \quad (\text{A.16})$$

where \mathbf{R} is the translation vector and $\mathcal{T}_{\mathbf{R}}$ translates any lattice vector \mathbf{r} to the position $\mathbf{r} + \mathbf{R}$. Because $[H, \mathcal{T}_{\mathbf{R}}] = 0$, it is possible to block diagonalize the Hamiltonian H in equation (A.1) using the eigenstates of $\mathcal{T}_{\mathbf{R}}$. This reduces the eigenvalue problem equation (A.9) of dimension $2M_x N_x \times 2M_y N_y$ to $M_x \times M_y$ eigenvalue equations of dimension $2N_x \times 2N_y$. Applying the magnetic Bloch theorem

$$\begin{pmatrix} u_{n\mathbf{k}}(\mathcal{T}_{\mathbf{R}}\mathbf{r}_i) \\ v_{n\mathbf{k}}(\mathcal{T}_{\mathbf{R}}\mathbf{r}_i) \end{pmatrix} = e^{-i\mathbf{k}\cdot\mathbf{R}} \begin{pmatrix} e^{-i(\pi/\Phi_0)\mathbf{A}(\mathbf{R})\cdot\mathbf{r}_i} u_{n\mathbf{k}}(\mathbf{r}_i) \\ e^{i(\pi/\Phi_0)\mathbf{A}(\mathbf{R})\cdot\mathbf{r}_i} v_{n\mathbf{k}}(\mathbf{r}_i) \end{pmatrix} \quad (\text{A.17})$$

block diagonalizes the BdG equation (A.10), where $\mathbf{k} = 2\pi\left(\frac{n_x}{M_x N_x}, \frac{n_y}{M_y N_y}\right)$, $u_{n\mathbf{k}}(\mathbf{r}_i) = u_{i n\mathbf{k}}$ and $v_{n\mathbf{k}}(\mathbf{r}_i) = v_{i n\mathbf{k}}$. Thus, we have to solve the following $2N_x \times 2N_y$ matrix equation for each \mathbf{k} value:

$$\sum_j \begin{pmatrix} H_{ij}^+(\mathbf{k}) & \Delta_{ij}(\mathbf{k}) \\ \Delta_{ij}^*(\mathbf{k}) & -H_{ij}^{-*}(\mathbf{k}) \end{pmatrix} \begin{pmatrix} u_{j n\mathbf{k}} \\ v_{j n\mathbf{k}} \end{pmatrix} = E_{n\mathbf{k}} \begin{pmatrix} u_{i n\mathbf{k}} \\ v_{i n\mathbf{k}} \end{pmatrix}, \quad (\text{A.18})$$

where

$$\Delta_{ij} = \frac{V_d}{4M_x M_y} \sum_{n\mathbf{k}} (u_{i n\mathbf{k}} v_{j n\mathbf{k}}^* + u_{j n\mathbf{k}} v_{i n\mathbf{k}}^*) \tanh\left(\frac{E_{n\mathbf{k}}}{2k_B T}\right), \quad (\text{A.19})$$

$$\langle n_{i\uparrow} \rangle = \frac{1}{M_x M_y} \sum_{n\mathbf{k}} |u_{i n\mathbf{k}}|^2 f(E_{n\mathbf{k}}), \quad (\text{A.20})$$

$$\langle n_{i\downarrow} \rangle = \frac{1}{M_x M_y} \sum_{n\mathbf{k}} |v_{i n\mathbf{k}}|^2 (1 - f(E_{n\mathbf{k}})). \quad (\text{A.21})$$

H_{ij} and Δ_{ij} are only \mathbf{k} dependent if i and j belong to different supercells. Then the back-mapping (see figure A.2) leads to an additional phase for the u 's and v 's according to

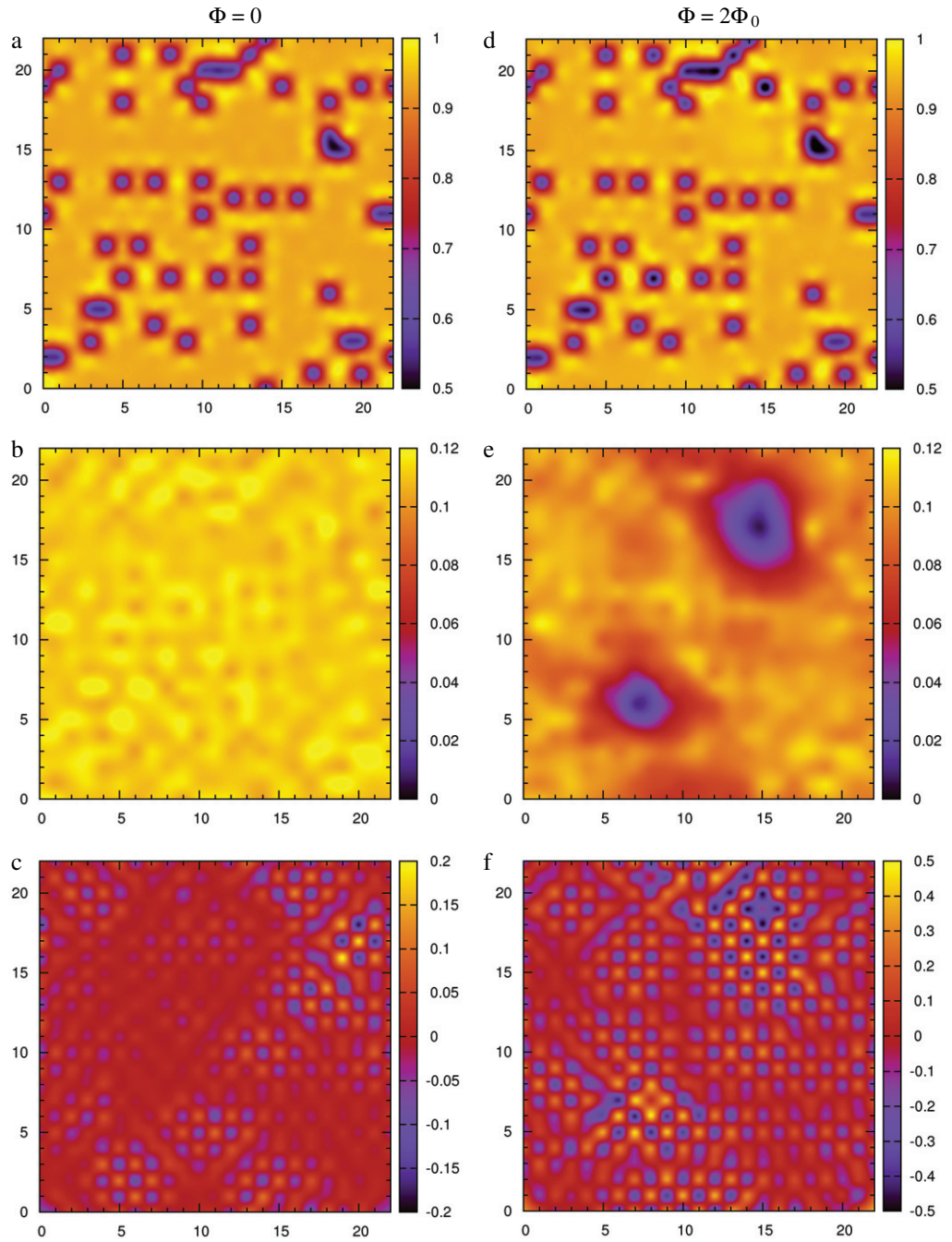


Figure A.3. Switching on an orbital magnetic field. (a–c) Zero-field data. (d–f) Finite-field data ($\Phi = 2\Phi_0$). (a, d) show the charge density $\langle n_i \rangle$, (b, e) the d-wave order parameter Δ_i^d and (c, f) the magnetization $\langle \sigma_i^z \rangle$ in real space. The same set of parameters is used here as in the rest of the paper, i.e. $x = 10\% = n_{\text{imp}}$, $U = 2.9t$, $V_{\text{imp}} = 1.3t$. These data were obtained at the lowest temperature $T = 0.025t$ we considered throughout the paper. Note the different scales in (c) and (f).

equation (A.18), which is assigned to the matrix elements $t_{ij}(\mathbf{k})$ and $\Delta_{ij}(\mathbf{k})$. To make sure that two magnetic translations commute, we have to choose the magnetic field such that its flux through every supercell is a multiple of $2\Phi_0$ [21, 40]. Hence $2\Phi_0$ provides a lower boundary for the magnetic flux threading each supercell, which corresponds to a supercell enclosing an area of e.g. $22a \times 22a$ to a magnetic field of about 59 T (we assumed a typical value for the in-plane lattice constant a in the cuprates of about $a = 3.8 \text{ \AA}$).

In order to make contact with neutron scattering experiments, we evaluate the magnetic structure factor $S(\mathbf{q})$. In homogeneous systems it is defined as

$$S(\mathbf{q}) = \frac{1}{N} \sum_i \langle \sigma_i^z \sigma_0^z \rangle e^{-i\mathbf{q} \cdot (\mathbf{r}_i - \mathbf{r}_0)}. \quad (\text{A.22})$$

We approximate the spin–spin correlation function by the following factorization:

$$\langle \sigma_i^z \sigma_0^z \rangle \rightarrow \langle \sigma_i^z \rangle \langle \sigma_0^z \rangle. \quad (\text{A.23})$$

Because the system that we are interested in is in general inhomogeneous, we have to sum over all lattice sites. Hence we find the expression

$$|M(\mathbf{q})|^2 = \frac{1}{N^2} \sum_{ij} \langle \sigma_i^z \rangle \langle \sigma_j^z \rangle e^{-i\mathbf{q} \cdot (\mathbf{r}_j - \mathbf{r}_i)}. \quad (\text{A.24})$$

This approximation of the magnetic structure factor is identical to the Fourier transform of the magnetization squared.

In figure A.3, the results for $\langle n_i \rangle$, Δ_i^d and $\langle \sigma_i^z \rangle$ are shown in zero field (left column) and in finite magnetic field (right column) for a typical impurity configuration. One can identify the location of the impurities by the point-like suppression of the charge density (top row). While the d-wave order parameter is nearly homogeneous in the zero-field case (see figure A.3(b)), one can clearly spot the positions of the two vortices where Δ_i^d is suppressed to zero in figure A.3(e). In comparison to the zero-field case, a finite orbital magnetic field leads to an additional reduction in the order parameter over the entire lattice. Finally, for the parameters used here, the zero-field case already contains impurity-induced AF order (see figure A.3(c)), which is significantly enhanced by switching on a magnetic field. The magnetization peaks near the vortex cores, but, due to the fact that strong type-II superconductors are penetrated by the field much beyond the cores, the magnetization is also enhanced in regions far away from the vortices, where the order parameter is nearly homogeneous. The SDW emerges due to the splitting of the Andreev bound state, as explained in greater detail in the main body of the paper.

References

- [1] Sachdev S 2003 *Rev. Mod. Phys.* **75** 913
- [2] Lake B *et al* 2002 *Nature* **415** 299
- [3] Haug D *et al* 2009 *Phys. Rev. Lett.* **103** 017001
- [4] Chang J *et al* 2008 *Phys. Rev. B* **78** 104525
- [5] Khaykovich B, Lee Y S, Erwin R W, Lee S-H, Wakimoto S, Thomas K J, Kastner M A and Birgeneau R J 2002 *Phys. Rev. B* **66** 014528
- [6] Khaykovich B, Wakimoto S, Birgeneau R J, Kastner M A, Lee Y S, Smeibidl P, Vorderwisch P and Yamada K 2005 *Phys. Rev. B* **71** 220508
- [7] Hoffman J E, Hudson E W, Lang K M, Madhavan V, Eisaki H, Uchida S and Davis J C 2002 *Science* **295** 466
- [8] Johnston D C 1989 *Phys. Rev. Lett.* **62** 957

- [9] Panagopoulos C, Tallon J L, Rainford B D, Xiang T, Cooper J R and Scott C A 2002 *Phys. Rev. B* **66** 064501
- [10] Niedermayer Ch, Bernhard C, Blasius T, Golnik A, Moodenbaugh A and Budnick J I 1998 *Phys. Rev. Lett.* **80** 3843
- [11] Kivelson S A, Bindloss I P, Fradkin E, Tranquada J M, Kapitulnik A and Howald C 2003 *Rev. Mod. Phys.* **75** 1201
- [12] Andersen B M, Hirschfeld P J, Kampf A P and Schmid M 2007 *Phys. Rev. Lett.* **99** 147002
- [13] Harter J W, Andersen B M, Bobroff J, Gabay M and Hirschfeld P J 2007 *Phys. Rev. B* **75** 054520
- [14] Tsuchiura H, Tanaka Y, Ogata M and Kashiwaya S 2000 *Phys. Rev. B* **64** 140501
- [15] Wang Z and Lee P A 2002 *Phys. Rev. Lett.* **89** 217002
- [16] Alloul H, Bobroff J, Gabay M and Hirschfeld P J 2009 *Rev. Mod. Phys.* **81** 45
- [17] Kimura H, Kofu M, Matsumoto M Y and Hirota K 2003 *Phys. Rev. Lett.* **91** 067002
- [18] Demler E, Sachdev S and Zhang Y 2001 *Phys. Rev. Lett.* **87** 067202
- [19] Wang Y and MacDonald A H 1995 *Phys. Rev. B* **52** R3876
- [20] Andersen B M, Bruus H and Hedegård P 2000 *Phys. Rev. B* **61** 6298
- [21] Zhu J-X and Ting C S 2001 *Phys. Rev. Lett.* **87** 147002
- [22] Chen Y and Ting C S 2002 *Phys. Rev. B* **65** 180513
- [23] Zhu J-X, Martin I and Bishop A R 2002 *Phys. Rev. Lett.* **89** 067003
- [24] Himeda A, Ogata M, Tanaka Y and Kashiwaya S 1997 *J. Phys. Soc. Japan* **66** 3367
- [25] Maggio-Aprile I *et al* 1995 *Phys. Rev. Lett.* **75** 2754
- [26] Pan S H, Hudson E W, Gupta A K, Ng K-W, Eisaki H, Uchida S and Davis J C 2000 *Phys. Rev. Lett.* **85** 1536
- [27] Pan S H, Hudson E W, Lang K M, Eisaki H, Uchida S and Davis J C 2000 *Nature* **403** 746
- [28] Doiron-Leyraud N, Proust C, LeBoeuf D, Levallois J, Bonnemaïson J-B, Liang R, Bonn D A, Hardy W N and Taillefer L 2007 *Nature* **447** 565
- [29] LeBoeuf D *et al* 2007 *Nature* **450** 533
- [30] Damascelli A, Hussain Z and Shen Z X 2003 *Rev. Mod. Phys.* **75** 473
- [31] Shender E F and Kivelson S A 1991 *Phys. Rev. Lett.* **66** 2384
- [32] Tranquada J M 2007 *Handbook of High-Temperature Superconductivity Theory and Experiment* ed J R Schrieffer (New York: Springer)
- [33] Watanabe I *et al* 2002 *Phys. Rev. B* **65** 180516
- [34] Adachi T, Yairi S, Takahashi K, Watanabe I and Nagamine K 2004 *Phys. Rev. B* **69** 184507
- [35] Robertson J A, Kivelson S A, Fradkin E, Fang A C and Kapitulnik A 2006 *Phys. Rev. B* **74** 134507
- [36] Del Maestro A, Rosenow B and Sachdev S 2006 *Phys. Rev. B* **74** 024520
- [37] Vojta M 2009 *Adv. Phys.* **58** 699
- [38] Ghosal A, Kallin C and Berlinsky A J 2002 *Phys. Rev. B* **66** 214502
- [39] Atkinson W A and Sonier J E 2008 *Phys. Rev. B* **77** 024514
- [40] Brown E 1964 *Phys. Rev. A* **133** 1038